Pomiary Automatyka Robotyka, ISSN 1427-9126, R. 27, Nr 3/2023, 95–106, DOI: 10.14313/PAR_249/95

Application of Impedance Control of the Free Floating Space Manipulator for Removal of Space Debris

Piotr Palma, Tomasz Rybus, Karol Seweryn
Space Research Centre, Polish Academy of Science (CBK PAN), Bartycka 18A, 00-716 Warsaw, Poland

Abstract: A broad and significant class of space debris can be mitigated by means of a satellite, capable of capturing a large non-cooperating object by using a robotized arm with a gripper. The capture operation typically comprises of an approach, a close-on manoeuvre, establishing contact between the robotic grappler arm and a suitable feature on the target satellite, and finally it is concluded when a positive mechanical connection is achieved by the gripper closed on that feature. The phase of establishing contact poses a critical challenge in this scenario, since the target typically will be tumbling with respect to the chaser satellite causing high forces on the gripper and the robotic arm. A family of control methods known collectively as impedance control is typically employed in terrestrial robots for tasks involving an interaction with an environment, especially the dynamic contact. In this work, we present the model-based impedance control applied to a robotic manipulator on a free floating base. The derivation of impedance control law for a robotic manipulator on a free floating satellite, involving Generalized Jacobian Matrix (GJM), is presented, followed by simulation results comparing the loads in the manipulator joints against a classical GJM-based Cartesian controller. The simulation results show that the impedance controlled free floating robotic manipulator completes the task of trajectory following amid contact with unknown target with lower torques in the robot joints.

Keywords: space manipulator; impedance control; nonholonomic; in-orbit servicing; debris removal, robotics

1. Introduction

The active debris removal and mitigation is an important priority of space exploration agencies [6]. An approximate measure of 10 cm in size is the threshold above which the object colliding with a spacecraft will generate further hundreds of objects of the disastrous size of 10 cm or larger. The highest risk is posed by large defunct satellites occupying important, and populated orbits like the geostationary or low Earth orbit [24]. The capability to physically intercept such objects opens a possibility to lower the risk of their collision with other satellites [10]. The captured defunct spacecraft or upper stages of launchers can be then manoeuvred away from the orbit where they posed a danger, using the propulsion and orbit control capabilities of the robotized satellite [4]. Some satellites whose main payload is still functioning while their orbit control functions are partly impaired (e.g. telecommunication satellites depleted of the orbit-correcting propellant) may be saved from becoming space debris if they can be attached to a servicer satellite capable of providing the manoeuvrability and orbit control functions for them. In either case, the success of the capture operations depends on the ability of the robotic arm to bring its end effector in contact with the object being captured and establish a mechanical connection between them.

Common scenarios for aforementioned establishment of the mechanical connection involve closing a gripper on a suitable mechanical feature of the object being intercepted. This requires manoeuvring the gripper by a robotic arm into a position on the feature and maintaining its position for the duration necessary of the gripper mechanism to form a positive geometric constraint e.g. by closing on a protruding, convex rigid feature e.g. like in [11] or around a rim of the separation ring or a thruster cone), or expanding inside a concave feature (e.g. inside a combustion chamber of a thruster like in [25]. The contact between the target moving with uncertain velocity and the rigid gripper of the end effector will result in abrupt and rapidly changing forces and torques being propagated from the end effector down through the joints of the arm to the base satellite. The proposed approach aims at providing the robotized satellite with means to control the dynamic stiffness of the point of interaction between its end effector and the object being intercepted while following the planned trajectory. For this purpose, the use of the impedance control paradigm is adopted to the context of a free floating space robot with

Autor korespondujący:
Piotr Palma, piotr@palmaline.pl, ppalma@cbk.waw.pl

Artykuł recenzowany
nadesłany 19.02.2023 r., przyjęty do druku 23.06.2023 r.

particular focus on the modelbased type of approach [21] and employing Generalized Jacobian Matrix in [23] which relates the end effector Cartesian velocity and angular rate to the time derivatives of configuration space variables of the robot arm on a free floating satellite. It takes into account the configuration-dependent changes of inertia across the whole chain of bodies comprising the robotic arm's links and the satellite. The impedance control is an established topic in terrestrial robotics literature [21, 17, 7–9]. The advances in the impedance control researches led to various implementation approaches established over the years, which are summarized in the comparative survey presented in [21]. The suitability of the impedance control to space robotic manipulation tasks has been recognized by research teams.

The impedance matching to the target satellite was proposed as a means to shape the dynamic properties of the capturing robotic arm of the intercepting satellite in [25]. The control of free floating space manipulators using Generalized Jacobian Matrix has established history [23] and numerous applications, including optimization [19], as well as evolution to multiple manipulators on a single satellite [3]. The work on application of impedance control to a satellite based robot [1] uses the Generalized Jacobian Matrix in the formulation of control. While it approaches formulation of model based impedance control, it focuses on the topics of computational complexity and uncertainty of the intercepted object. The approach to compliance control of satellite manipulator using force controller is proposed in [20].

The goal of our research is to formulate the model-based impedance controller for a satellite model operating in three dimensional space, as a continuation of work of the authors done on a model in 2D space [12]. The second goal is to simulate the controller's performance in comparison with a Cartesian controller used as a benchmark in space robotics control research in [15] with focus on the joint loads and disturbance of the satellite generated by the external force exerted on the manipulator end effector. The importance of the amplitude and time characteristics of the disturbance and torque loads which the joints have to counteract by their drives is important for establishing the operational envelope of the drives and their control performance. This is especially important in the space applications, where allowable mass and power are stringent constraints for robotic hardware. Slower load transients with lower peaks naturally allow for less powerful, lighter drives, and ease the bandwidth requirements on control compared to abrupt peaks in torque loads.

The text is organized as follows: In the section 2 the mathematical model of the system is elaborated. Section 2.2 derives the equations of motion of the space robot. A short discussion of types of impedance control is laid out as the basis for selection of the model-based impedance control law in section 3.1 followed by the derivation of the model based impedance control for the free floating robot in section 3.2. A classical, GJM-based Cartesian control of the space robot is introduced in section 2.3 as a benchmark controller for comparison with the impedance one. In the section 4, the simulation environment for the space robotics platforms is used to simulate a 7-DoF robotic arm on a free floating satellite base attempting to follow a planned trajectory involving contact with another free floating body. The satellite based robot is controlled by the impedance controller and by a benchmark Cartesian controller. Both sharing the same GJM. Section 4 presents and discusses the results obtained with the impedance controller comparing them with simulation results of the same robot controlled by a classical Cartesian controller.

2. Mathematical Model of the Space Robot

2.1. The Nonholonomic nature of a free floating space robot

The free floating satellite equipped with manipulator arm exhibits nonholonomic properties as the angular momentum of the system consisting of the satellite and manipulator chain is not integrable [13]. The presented control method does not address the nonholonomic aspects of the trajectory planning and tracking, unlike e.g. [22], but the simulation cases are selected such that the simulated trajectories are unlikely to evolve into singular ones.

2.2. Equations of motion of a free floating space robot

The satellite equipped with robotic arm is modelled as a multibody system. It is described using the coordinate systems depicted in Figure 1.

The satellite centre of mass is defined in the inertial reference frame by vector $\mathbf{r}_s$. The end effector is at $\mathbf{r}_{ee}$. The base of the first joint of the robotic arm is displaced from the satellite centre of mass by $\mathbf{r}_q$. Each link has the length vector $\mathbf{l}$ pointing to the next joint coordinate frame.

2.2.1. Kinematics of the free floating space robot

In this subsection, the standard description of the manipulator kinematic equations is recalled after [23, 15]. In the inertial reference system, the satellite's center of mass position $\boldsymbol{r}_s$ is

$$\boldsymbol{r}_s = [(r_s)_x \quad (r_s)_y \quad (r_s)_z]^{\mathrm{T}}, \tag{1}$$

The satellite's orientation $\boldsymbol{\theta}_s$ is expressed using Euler angles as follows:

$$\boldsymbol{\theta}_s = [\psi \quad \phi \quad \theta]^{\mathrm{T}}, \tag{2}$$

The series-type manipulator with n joints is described by a vector of configuration variables corresponding to the angles of each joint:

$$\boldsymbol{\theta} = [\theta_1 \quad \ldots \quad \theta_n]^{\mathrm{T}}. \tag{3}$$

The vector of generalised coordinates $\boldsymbol{q}_p$, describing the system of satellite base and manipulator is assembled from definitions (1) (2) and (3)

$$\boldsymbol{q}_p = \begin{bmatrix} \boldsymbol{r}_s \\ \boldsymbol{\Theta}_s \\ \boldsymbol{\theta} \end{bmatrix} \tag{4}$$

The differentiation of the state vector yields the following expression, where $\boldsymbol{T}_\theta$ transforms the angular velocities to the time derivatives of the Euler angles:

$$\boldsymbol{q}_v = \begin{bmatrix} \dfrac{\mathrm{d}\boldsymbol{r}_s}{\mathrm{d}t} \\ T_{\boldsymbol{\theta}}^{-1} \dfrac{\mathrm{d}\boldsymbol{\Theta}_s}{\mathrm{d}t} \\ \dfrac{\mathrm{d}\boldsymbol{\theta}}{\mathrm{d}t} \end{bmatrix} = \begin{bmatrix} \boldsymbol{v}_s \\ \boldsymbol{\omega}_s \\ \dot{\boldsymbol{\theta}} \end{bmatrix} \tag{5}$$

The position vector of the end effector in the inertial frame is determined by the sum of positions of the links of the robot manipulator and the satellite position:

$$\boldsymbol{r}_{ee} = \boldsymbol{r}_s + \boldsymbol{r}_q + \sum_{i=1}^{n} \boldsymbol{l}_i \tag{6}$$

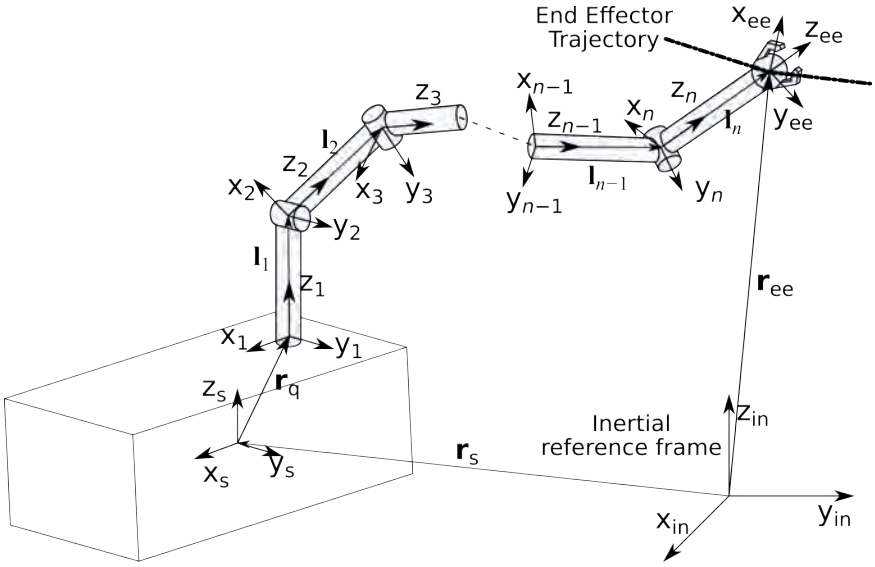

Fig. 1. Schematic depiction of the satellite-based robotic arm with reference frames and defining geometrical parameters
Rys. 1. Schematyczne przedstawienie robota kosmicznego z zaznaczonymi układami współrzędnych i kluczowymi prametrami geometrycznymi

as depicted in Figure 1. By taking the time derivative of the expression for position vector, we arrive with the end effector velocity in the Cartesian inertial frame:

$$\boldsymbol{v}_{ee} = \boldsymbol{v}_s + \boldsymbol{\omega}_s \times \left(\boldsymbol{r}_{ee} - \boldsymbol{r}_s\right) + \sum_{i=1}^{n} \left[\boldsymbol{k}_i \times \left(\boldsymbol{r}_{ee} - \boldsymbol{r}_i\right)\right] \dot{\theta}_l \tag{7}$$

For an i-th joint, $\boldsymbol{k}_i$ represents the unit vector of the rotation axis and $\dot{\theta}_l$ is its angular rate, while $\boldsymbol{r}_i$ represents the position of the ith kinematic pair. The angular velocity of the end effector is simply:

$$\boldsymbol{\omega}_{ee} = \boldsymbol{\omega}_s + \sum_{i=1}^{n} \boldsymbol{k}_i \dot{\theta}_l \tag{8}$$

Having arrived at the kinematic expressions for the velocities the model of dynamics of the satellite manipulator system can be formulated.

2.2.2. Dynamics of the space robot

This section introduces the dynamics of a full (non-free floating) space robot without nonholonomic constraints. The reaction forces and torques acting on the system are following:

$$\boldsymbol{Q} = \begin{bmatrix} \boldsymbol{F}_s \\ \boldsymbol{H}_s \\ \boldsymbol{T} \end{bmatrix} \tag{9}$$

were $\boldsymbol{F}_s$ and $\boldsymbol{H}_s$ are the forces and torques acting on the satellite base center of mass. Elements of the vector $\boldsymbol{T}$ are the torques in the joints of the robotic arm. The derivation of the generalized equations of motion for the satellite equipped with robotic manipulator using the Lagrangian equations of the second kind take the following form [19]:

$$\boldsymbol{Q} = \boldsymbol{M}\left(\boldsymbol{q}_p\right)\dot{\boldsymbol{q}}_v + \boldsymbol{C}\left(\dot{\boldsymbol{q}}_p, \boldsymbol{q}_p\right)\boldsymbol{q}_v \tag{10}$$

The mass matrix $\boldsymbol{M}$ [23, 15] for the general case is:

$$\boldsymbol{M} = \begin{bmatrix} \boldsymbol{A} & \boldsymbol{B} & \boldsymbol{D}_M \\ \boldsymbol{B}^{\mathrm{T}} & \boldsymbol{E}_M & \boldsymbol{F}_M \\ \boldsymbol{D}_M^{\mathrm{T}} & \boldsymbol{F}_M^{\mathrm{T}} & \boldsymbol{N} \end{bmatrix} \tag{11}$$

The velocity dependent effects are modelled by the Coriolis matrix whose entries have the following form [5]:

$$c_{ij} = \sum_{k=1}^{n} \frac{1}{2}\left(\frac{\mathrm{d}}{\mathrm{d}q_k} m_{ij} + \frac{\mathrm{d}}{\mathrm{d}q_j} m_{ik} - \frac{\mathrm{d}}{\mathrm{d}q_i} m_{jk}\right)\dot{q}_k \tag{12}$$

where the $m_{ij} \in \boldsymbol{M}\left(q_p\right)$ and $i, j, k = 1, \ldots, n$. The sub-matrices of the mass matrix (11) are:

$$\boldsymbol{A} = \left(\boldsymbol{m}_s + \sum_{i=1}^{n}\left(\boldsymbol{m}_i\right)\right)\boldsymbol{I} \tag{13}$$

$$\boldsymbol{B} = \left(\boldsymbol{m}_s + \sum_{i=1}^{n}\left(\boldsymbol{m}_i\right)\right)\tilde{\boldsymbol{r}}_{s\_q} \tag{14}$$

$$\boldsymbol{D}_M = \sum_{i=1}^{n}\left(\boldsymbol{m}_i \boldsymbol{J}_{Ti}\right) \tag{15}$$

$$\boldsymbol{E}_M = \boldsymbol{I}_s + \sum_{i=1}^{n}\left(\boldsymbol{I}_i + \boldsymbol{m}_i \tilde{\boldsymbol{r}}_{i\_s}^{\mathrm{T}} \tilde{\boldsymbol{r}}_{i\_s}\right) \tag{16}$$

$$\boldsymbol{F}_M = \sum_{i=1}^{n}\left(\boldsymbol{I}_i \boldsymbol{J}_{Ri} + \boldsymbol{m}_i \tilde{\boldsymbol{r}}_{i\_s} \boldsymbol{J}_{Ti}\right) \tag{17}$$

$$\boldsymbol{N} = \sum_{i=1}^{n}\left(\boldsymbol{J}_{Ri}^{\mathrm{T}} \boldsymbol{I}_i \boldsymbol{J}_{Ri} + \boldsymbol{m}_i \boldsymbol{J}_{Ti}^{\mathrm{T}} \boldsymbol{J}_{Ti}\right) \tag{18}$$

With $\boldsymbol{r}_{s\_q} = \boldsymbol{r}_s - \boldsymbol{r}_q$, $\boldsymbol{r}_{i\_s} = \boldsymbol{r}_{m,i} - \boldsymbol{r}_s$ where $\boldsymbol{r}_{m,i}$ is the position of centre of mass of i-th link, while the $\boldsymbol{J}_{Ti}$, $\boldsymbol{J}_{Ri}$ are the translational and rotational components of a Jacobian of the i-th link of the manipulator (relating the joint velocities to the end effector position expressed in the coordinate frame of the base of the manipulator). The tilde symbol ~ denotes a skew symmetric matrix of a vector. The matrix $\boldsymbol{I}_s$ is the satellite inertia matrix, $\boldsymbol{I}_i$ denotes the inertia matrices of each link and $\boldsymbol{I}$ is an identity matrix.

2.2.3. Free floating space manipulator

In case of a free floating manipulator system, being the scope of this research, the above formulation of the kinematics and dynamics equations change. The manipulator's angular momentum is described as follows:

$$\boldsymbol{L} = \boldsymbol{L}_0 + \boldsymbol{r}_s \times \boldsymbol{P} \tag{19}$$

With $\boldsymbol{L}_0$ being the initial angular momentum and $\boldsymbol{P}$ being the linear momentum for which the following relationship holds:

$$\begin{bmatrix} \boldsymbol{L} \\ \boldsymbol{P} \end{bmatrix} = \boldsymbol{H}_2 \begin{bmatrix} \boldsymbol{v}_s \\ \boldsymbol{w}_s \end{bmatrix} + \boldsymbol{H}_3 \dot{\boldsymbol{\theta}} = \boldsymbol{0} \tag{20}$$

with

$$\boldsymbol{H}_2 = \begin{bmatrix} \boldsymbol{A} & \boldsymbol{B} \\ \boldsymbol{B}^{\mathrm{T}} + \tilde{\boldsymbol{r}}_s \boldsymbol{A} & \boldsymbol{E} + \tilde{\boldsymbol{r}}_s \boldsymbol{B} \end{bmatrix} \tag{21}$$

$$\boldsymbol{H}_3 = \begin{bmatrix} \boldsymbol{D}_M \\ \boldsymbol{F}_M + \tilde{\boldsymbol{r}}_s \boldsymbol{D}_M \end{bmatrix} \tag{22}$$

The system is free floating and there is no exchange of momentum and angular momentum with the environment, hence the equation (20) is equated to zero. The relationship between the angular velocities of the joints of the space robot and the linear and angular velocity of the end effector $\boldsymbol{v}_{ee}$, $\boldsymbol{\omega}_{ee}$ are given by:

$$\begin{bmatrix} \boldsymbol{v}_{ee} \\ \boldsymbol{\omega}_{ee} \end{bmatrix} = \left(\boldsymbol{J}_M - \boldsymbol{J}_S \boldsymbol{H}_2^{-1} \boldsymbol{H}_3 \right) \dot{\boldsymbol{\theta}} \tag{23}$$

Where finally the Generalized Jacobian Matrix (GJM) emerges as $\boldsymbol{J}_D$:

$$\boldsymbol{J}_D = \left(\boldsymbol{J}_M - \boldsymbol{J}_S \boldsymbol{H}_2^{-1} \boldsymbol{H}_3 \right) \tag{24}$$

The Jacobian $\boldsymbol{J}_M$ is a standard manipulator Jacobian mentioned earlier and the satellite Jacobian $\boldsymbol{J}_S$ is defined as:

$$\boldsymbol{J}_S = \begin{bmatrix} \boldsymbol{I} & \tilde{\boldsymbol{r}}_{ees}^{\mathrm{T}} \\ \boldsymbol{0} & \boldsymbol{I} \end{bmatrix} \tag{25}$$

Where $\tilde{\boldsymbol{r}}_{ees} = \boldsymbol{r}_{ee} - \boldsymbol{r}_s$ expressed in a matrix form.

2.2.4. Dynamics of the free floating manipulator

The center of mass of the satellite-arm system remains constant under the assumption of no momentum exchange with environment and by neglecting the orbital motion but the base is free to change its orientation and position in the inertial reference frame. In such case the vector $\boldsymbol{q}_p$ in (4) contains only the joint angles.

$$\begin{aligned} \boldsymbol{q}_p &= \boldsymbol{\theta} \\ \boldsymbol{q}_v &= \dot{\boldsymbol{\theta}} \end{aligned} \tag{26}$$

The vector of generalized forces becomes:

$$\boldsymbol{Q}_m = \boldsymbol{T} = \left[T_1, T_2 \ldots T_n \right]^{\mathrm{T}} \tag{27}$$

By applying the approach presented in the paper [14] and using constrained Lagrangian formulation, the mass matrix becomes:

$$\boldsymbol{M}_m(\boldsymbol{q}) = \boldsymbol{N} - \begin{bmatrix} \boldsymbol{D}_M \\ \boldsymbol{F}_M \end{bmatrix}^{\mathrm{T}} \begin{bmatrix} \boldsymbol{A} & \boldsymbol{B} \\ \boldsymbol{B}^{\mathrm{T}} & \boldsymbol{E} \end{bmatrix}^{-1} \begin{bmatrix} \boldsymbol{D}_M \\ \boldsymbol{F}_M \end{bmatrix} \tag{28}$$

2.3. Basic Cartesian controller for free floating robot

A simple control strategy for a trajectory following task in Cartesian coordinates can be realized for a space robot using the GJM. This strategy will then be used by us as a benchmark for the actual impedance controller following [15].

The dynamic Jacobian relates the velocity space to joint space so a simple controller computing the joint velocities can be expressed as in (24). It can be used to find joint velocities $\dot{\boldsymbol{\theta}}_{cont}$ minimizing the deviation $\boldsymbol{e}_v$ between the intended and actual velocity as follows:

$$\dot{\boldsymbol{\theta}}_{cont} = \boldsymbol{J}_D^{\dagger} \boldsymbol{e}_v \tag{29}$$

Since the planned trajectory is typically not defined in the velocity space but rather in the position space, we use the approximation of the velocity error $\boldsymbol{e}_v$ by the position and orientation error $\boldsymbol{e}_p$ multiplied by some gain matrix $\boldsymbol{G}_{ee}$. The joint control torques defined by the simple Cartesian trajectory following controller are given by:

$$\boldsymbol{T} = \boldsymbol{G}_{\dot{\boldsymbol{\theta}}} \left(\boldsymbol{J}_D^{\dagger} \boldsymbol{G}_{ee} \boldsymbol{e}_p - \dot{\boldsymbol{\theta}} \right) \tag{30}$$

Where $\boldsymbol{G}_{\dot{\boldsymbol{\theta}}}$ is the gain matrix converting the difference between $\dot{\boldsymbol{\theta}}_{contr}$ and current joint angular velocities $\dot{\boldsymbol{\theta}}$ to the control torque.

3. The Impedance Control

Impedance control [21, 7, 8] is a paradigm which aims to achieve a desired characteristics of the interaction between the robot and its environment. It draws from the long recognized analogies between electrical and mechanical building blocks of dynamic systems and became an important toolbox for modelling robotics interacting with environment and humans, cooperative robotics, exoskeletons etcetera. Impedance describes the dynamic behaviour of the system at its interaction port with the environment which is the end effector in case of most robotic manipulators.

The impedance is fundamentally a relationship between the input "flow variables" F like velocity or electric current and output "effort variables" $\dot{X}$ – force or voltage. In the Laplace domain this can be written as the following ratio:

$$Z(s) = \frac{F(s)}{\dot{X}(s)} \tag{31}$$

Since most robotic tasks involving interaction with an environment are naturally defined in coordinates relative to the environment, it is useful to replace the $\dot{X}(s)$ with relative displacement $sX_r(s)$. Specifically, the relative displacement is understood as the difference between the current actual position of the interaction port X relative to the intended one, often referred to as the "virtual" trajectory X_0 [7].

$$X_r = X - X_0 \tag{32}$$

The virtual trajectory is useful in its generality since it can be defined in terms of position space as, as well as velocity or acceleration spaces and need not be within the reachable space of the manipulator [8]. In a basic form, the mechanical impedance is typically described to be composed of elements which exhibit an inertia-like or mass – like behavior represented below as M_d, damping-like behavior described by D and elastic-like behavior described by matrix E.

$$Z(s) = M_d s + D + E/s \tag{33}$$

Substituting (32) and (33) into (31), rearranging terms and taking the inverse Laplace transform gives the time-domain differential equation describing the interaction point forces $\boldsymbol{F}$ as a function of the difference between current and virtual trajectory, parametrized by the desired inertia parameters:

$$\boldsymbol{M}_d\left(\ddot{\boldsymbol{x}} - \ddot{\boldsymbol{x}}_0\right) + \boldsymbol{D}\left(\dot{\boldsymbol{x}} - \dot{\boldsymbol{x}}_0\right) + \boldsymbol{E}\left(\boldsymbol{x} - \boldsymbol{x}_0\right) = \boldsymbol{F}(t) \tag{34}$$

The above basic formulation of a generic impedance control law can be described from the point of view of the environment as "hiding" the natural dynamics of the manipulator and exposing only the desired dynamics at the interaction port. At the implementation level there are numerous ways by which the dynamic behavior of the robot's interaction port can be shaped. There exist purely mechanical methods like springs and dampers or exploiting the redundancies of the manipulator to achieve different inertial properties by the virtue of their dependence on the manipulator's configuration shown in [7, 8]. The software based methods rely on using control strategies which reproduces the dynamic behavior with robot's actuators based on the loop closed via sensors. Three important types of software approaches to impedance implementation discussed in [21] are:

- Position based approach, where typically the controller's outer loop gives the desired position based on the desired impedance parameters and feedback information about interaction force, and inner loop tracks the position simply as a position servo.
- Torque/force based approach, where instead of the position, the outer loop commands the torque or force and the inner loop is the torque/force servo.
- Model based approach, which fundamentally differs from the previous two, because it uses the known manipulator dynamics and substitutes into it the desired dynamics described by the impedance parameters.

An exhaustive discussion and comparison of the above methods is presented in [21]. In this work we propose the use of Cartesian, model-based impedance controller to a space robot on a free floating satellite platform.

3.1. Cartesian impedance control

In this section we briefly recall the Cartesian impedance control [7, 8] and show how the dynamics model of the free floating satellite robot is incorporated into the control law. Note that in this chapter θ and ω are not related to the satellite from previous chapters.

A general robotic manipulator dynamic is modelled by the configuration dependent inertia $\boldsymbol{I}(\boldsymbol{\theta})$, configuration and velocity dependent inertial coupling between the links e.g. Coriolis and centrifugal effects $\boldsymbol{C}_c(\boldsymbol{\theta}, \boldsymbol{\omega})$, and $\boldsymbol{V}_c(\boldsymbol{\theta})$ the velocity dependent terms e.g. the viscous friction. The static forces $\boldsymbol{S}(\boldsymbol{\theta})$ like gravitational loads are assumed to be zero, since the application we are discussing is set in microgravity context of on-orbit operation. The manipulator control torques are denoted as $\boldsymbol{T}_{act}$ and $\boldsymbol{T}_{int}$, $\boldsymbol{F}_{int}$ are the torques and force due to interaction at the interface.

$$\boldsymbol{I}(\boldsymbol{\theta})\frac{\mathrm{d}\boldsymbol{\omega}}{\mathrm{d}t} + \boldsymbol{C}_c(\boldsymbol{\theta},\boldsymbol{\omega}) + \boldsymbol{V}_c(\boldsymbol{\omega}) + \boldsymbol{S}(\boldsymbol{\theta}) = \boldsymbol{T}_{act} + \boldsymbol{T}_{int} \tag{35}$$

The desired behavior in Cartesian space can be expressed as follows:

$$\frac{\mathrm{d}\boldsymbol{V}}{\mathrm{d}t} = \boldsymbol{M}_d^{-1}\boldsymbol{E}\left(\boldsymbol{X}_0 - \boldsymbol{X}\right) + \boldsymbol{M}_d^{-1}\boldsymbol{D}\left(\dot{\boldsymbol{X}}_0 - \dot{\boldsymbol{X}}\right) + \boldsymbol{M}_d^{-1}\boldsymbol{F}_{int} \tag{36}$$

With use of standard manipulator Jacobian, the transformation between the Cartesian and joint space follows:

$$\frac{\mathrm{d}\boldsymbol{V}}{\mathrm{d}t} = \boldsymbol{J}(\boldsymbol{\theta})\frac{\mathrm{d}\boldsymbol{\omega}}{\mathrm{d}t} + \boldsymbol{G}(\boldsymbol{\theta},\boldsymbol{\omega}) \tag{37}$$

$$\boldsymbol{G}(\boldsymbol{\theta},\boldsymbol{\omega}) = \frac{\mathrm{d}\left[\boldsymbol{J}(\boldsymbol{\theta})\right]}{\mathrm{d}t}\boldsymbol{\omega} \tag{38}$$

$$\frac{\mathrm{d}\boldsymbol{\omega}}{\mathrm{d}t} = \boldsymbol{J}^{-1}(\boldsymbol{\theta})\left[\frac{\mathrm{d}\boldsymbol{V}}{\mathrm{d}t} - \boldsymbol{G}(\boldsymbol{\theta},\boldsymbol{\omega})\right] \tag{39}$$

And the Cartesian impedance control law takes the form:

$$\begin{aligned}
&\boldsymbol{T}_{act} = \boldsymbol{I}(\boldsymbol{\theta})\boldsymbol{J}^{-1}(\boldsymbol{\theta})\boldsymbol{M}_d^{-1}\boldsymbol{E}\left[\boldsymbol{X}_0 - \boldsymbol{X}\right] + \boldsymbol{S}(\boldsymbol{\theta}) && \text{(position terms)}\\
&+\boldsymbol{I}(\boldsymbol{\theta})\boldsymbol{J}^{-1}(\boldsymbol{\theta})\boldsymbol{M}_d^{-1}\boldsymbol{D}\left[\dot{\boldsymbol{X}}_0 - \boldsymbol{V}\right] + \dot{\boldsymbol{X}}_c(\boldsymbol{\omega}) && \text{(velocity terms)}\\
&+\boldsymbol{I}(\boldsymbol{\theta})\boldsymbol{J}^{-1}(\boldsymbol{\theta})\boldsymbol{M}_d^{-1}\boldsymbol{F}_{int} - \boldsymbol{J}^{\mathrm{T}}(\boldsymbol{\theta})\boldsymbol{F}_{int} && \text{(force interaction terms)}\\
&-\boldsymbol{I}(\boldsymbol{\theta})\boldsymbol{J}^{-1}(\boldsymbol{\theta})\boldsymbol{G}(\boldsymbol{\theta},\boldsymbol{\omega}) + \boldsymbol{C}_c(\boldsymbol{\theta},\boldsymbol{\omega}) && \text{(inertial coupling terms)}
\end{aligned} \tag{40}$$

3.2. Free floating platform based space robot under Cartesian impedance control

In case of the free floating satellite platform equipped with a robotic manipulator, the Jacobian in (35)−(40) is replaced with its dynamic counterpart given by (24). The mass matrix (28) encodes the configuration dependent inertial properties of the manipulator and base. Combining the above we arrive at the following expression:

$$\begin{aligned}
\boldsymbol{T} = &\boldsymbol{M}_m(\boldsymbol{\theta})\boldsymbol{J}_D^{-1}(\boldsymbol{\theta})\boldsymbol{M}_d^{-1}\boldsymbol{E}\left[\boldsymbol{X}_0 - \boldsymbol{X}\right]\\
&+\boldsymbol{M}_m(\boldsymbol{\theta})\boldsymbol{J}_D^{-1}(\boldsymbol{\theta})\boldsymbol{M}_d^{-1}\boldsymbol{D}\left[\dot{\boldsymbol{X}}_0 - \dot{\boldsymbol{X}}\right]\\
&+\boldsymbol{M}_m(\boldsymbol{\theta})\boldsymbol{J}_D^{-1}(\boldsymbol{\theta})\boldsymbol{M}_d^{-1}\boldsymbol{F}_{int} - \boldsymbol{J}_D^{\mathrm{T}}(\boldsymbol{\theta})\boldsymbol{F}_{int}\\
&-\boldsymbol{M}_m(\boldsymbol{\theta})\boldsymbol{J}_D^{-1}(\boldsymbol{\theta})\boldsymbol{G}\left(\boldsymbol{q}_p,\boldsymbol{q}_v\right) + \boldsymbol{C}\left(\boldsymbol{q}_p,\boldsymbol{q}_v\right)\boldsymbol{q}_v
\end{aligned} \tag{41}$$

The equation relates the driving torques $\boldsymbol{T}$ of the joints to the end effector's deviation from the virtual trajectory, parametrized by desired impedance terms, in essence expressing the Cartesian impedance control law for the robot on a free floating satellite base.

The driving torque $\boldsymbol{T}$ as well as the effects of the force $\boldsymbol{F}_{int}$ acting on the end effector are introduced into the satellitemanipulator dynamics equation right hand side.

$$\boldsymbol{M}\left(\boldsymbol{q}_p\right)\dot{\boldsymbol{q}}_v + \boldsymbol{C}\left(\dot{\boldsymbol{q}}_p,\boldsymbol{q}_v\right)\dot{\boldsymbol{q}}_v = \begin{bmatrix}\boldsymbol{F}_S\\ \boldsymbol{H}_s\\ \boldsymbol{T}\end{bmatrix} + \begin{bmatrix}\boldsymbol{0}\\ \boldsymbol{0}\\ \boldsymbol{J}_M\left(\boldsymbol{q}_p\right)^{\mathrm{T}}\boldsymbol{F}_{int}\end{bmatrix} \tag{42}$$

The following chapter presents the simulation of the system (42) under control (41).

4. Simulation

4.1. Simulation parameters and configuration

The simulation of a free floating space robot with the proposed control method was performed using the simulation tool developed at the Space Research Center of the Polish Academy of Sciences and used in numerous research [16, 2, 3]. The robot

arm configuration is 7-DoF and is depicted in Figure 2 and the block diagram on Figure 3.

The system has the mass and geometrical parameters as listed in Table 1.

Table 1. Geometric and mass properties of the simulated robot
Tabela 1. Kluczowe parametry masowe i geometryczne manipulatora symulowanego robota

Link	Length [m]	Mass [kg]	Inertia [kg · m²] (dominant about the joint axis)
1	0.28	1.60	0.004
2	0.2	4.20	1.25
3	0.6	1.60	0.004
4	0.6	4.40	1.14
5	0.2	1.60	0.004
6	0.1	1.60	0.008
7	0.1	0.19	1e-04

The satellite base mass is 100 kg and has inertia $I_{xx} = 2.8$, $I_{yy} = 6.0$, $I_{zz} = 7.4$ kg·m². The manipulator mounting point is shifted from the centre of mass of the satellite by [200 100 400] mm. Model uncertainty was not the subject of this study and the simulation approach allows to assume ideal model. In a nonideal setting the uncertainty of the model of the satellite would affect the control law in various ways: One would affect the accuracy, which can be assessed using e.g. Monte Carlo methods with model parameter randomization around expected ranges. Another aspect is the model uncertainty impact on the numerical quality of the matrix inversions. This would be more important in a hypothetical embedded controlled implementing the control law, with lower precision than MATLAB environment used for this study.

4.2. Contact model

The external force $\boldsymbol{F}_{int}$ acting on the interface of the end effector is simulated using the following simplified spherical contact model (Fig. 4). The contact force acts along the line connecting the centers of two spheres. One sphere simulates the end effector, while the second sphere simulates a target with uniform mass distribution.

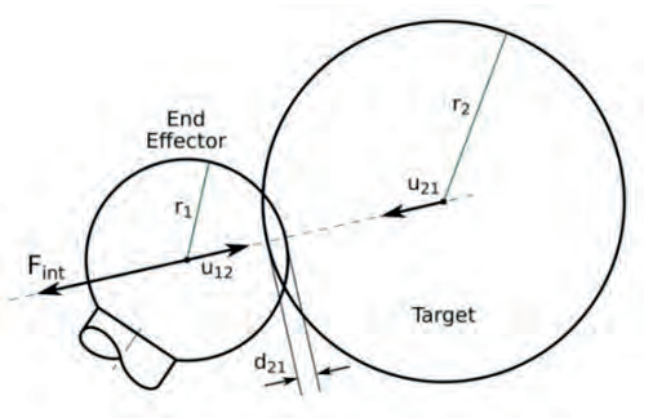

Fig. 4. Simplified contact model used in the simulation (not to scale)
Rys. 4. Schematyczne przedstawienie modelu kontaktu użytego w symulacji

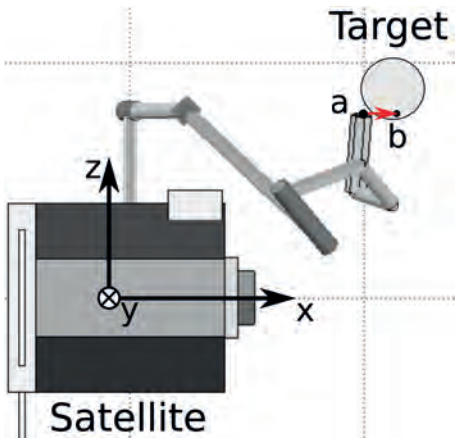

Fig. 2. Visualization of the simulated satellite robot, target and intended end effector trajectory depicted by the red arrow a-b
Rys. 2. Schemat symulowanego scenariusza wejścia w kontakt końcówki roboczej manipulatora robota kosmicznego z obiektem. Śledzona trajektoria oznaczona jest strzałką a-b

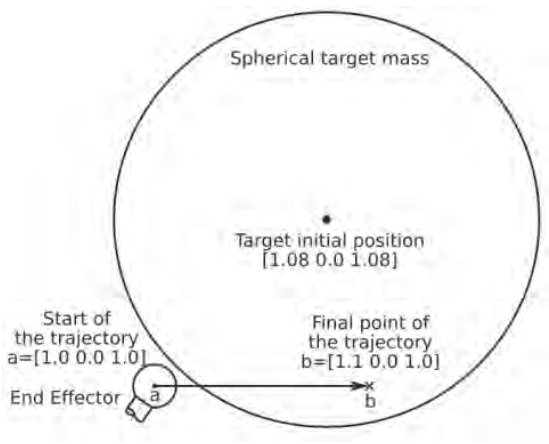

Fig. 5. Initial configuration of the robot end effector with relation to the target mass
Rys. 5. Szczegółowe przedstawienie początkowego położenia końcówki roboczej i obiektu-celu oraz śledzonej trajektorii w symulowanym scenariuszu

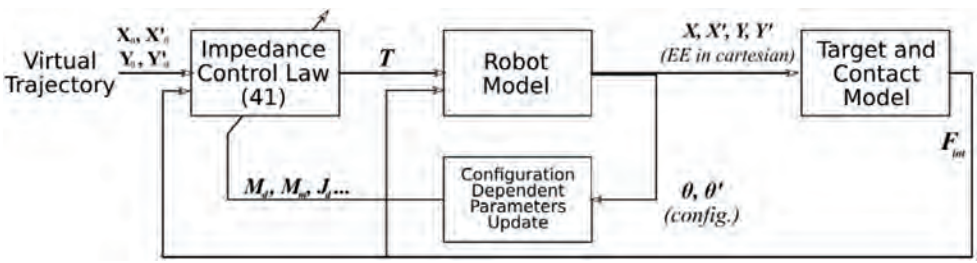

Fig. 3. Block diagram of the simulated system under control
Rys. 3. Schemat blokowy symulowanego układu, na który składa się robot satelitarny, jego prawo sterowania oraz obiekt-cel

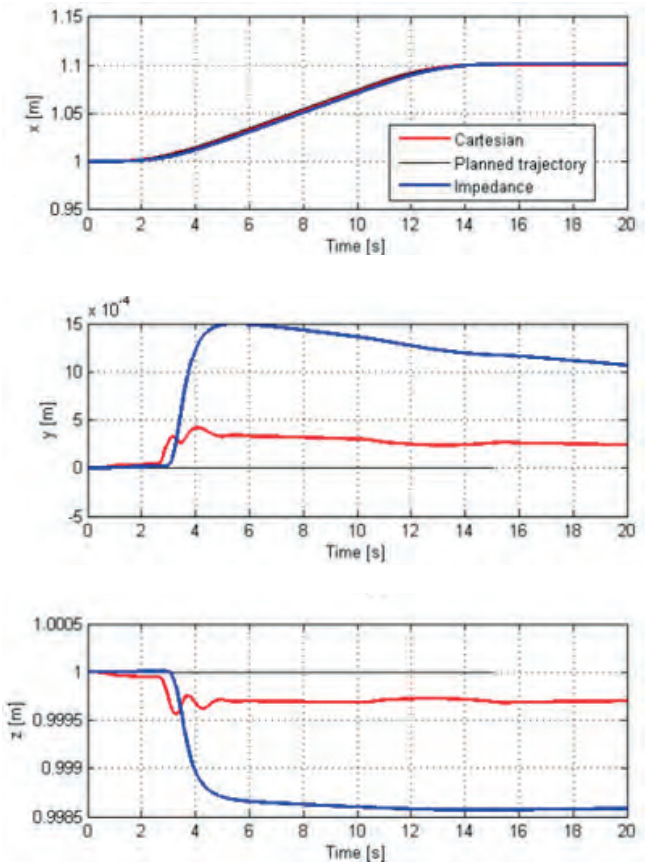

Fig. 6. Trajectory tracking in case of contact with 5 kg target
Rys. 6. Rezultat symulacji śledzenia trajektorii w przypadku kontaktu z obiektem-celem o masie 5 kg

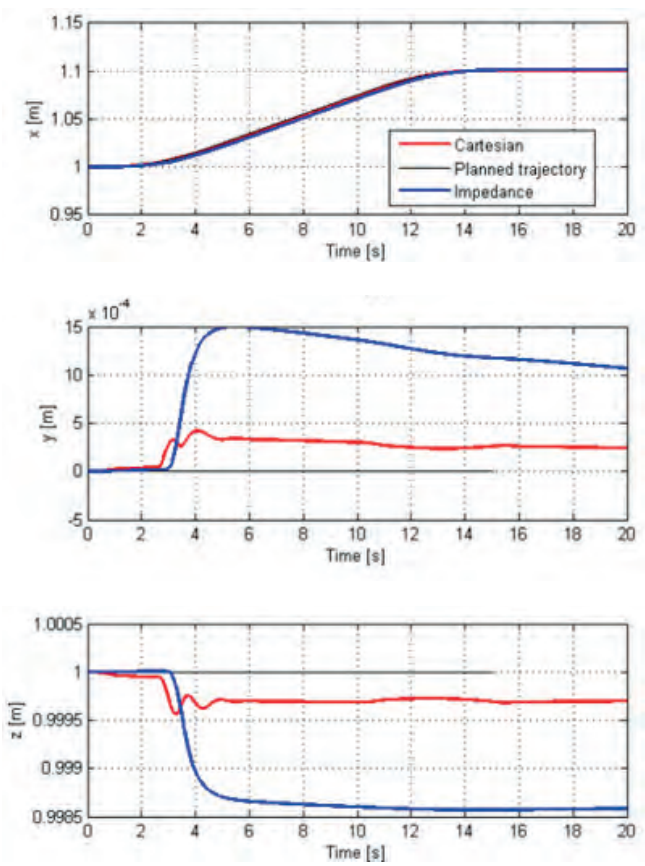

Fig. 7. Trajectory tracking in case of contact with 50 kg target
Rys. 7. Rezultat symulacji śledzenia trajektorii w przypadku kontaktu z obiektem-celem o masie 50 kg

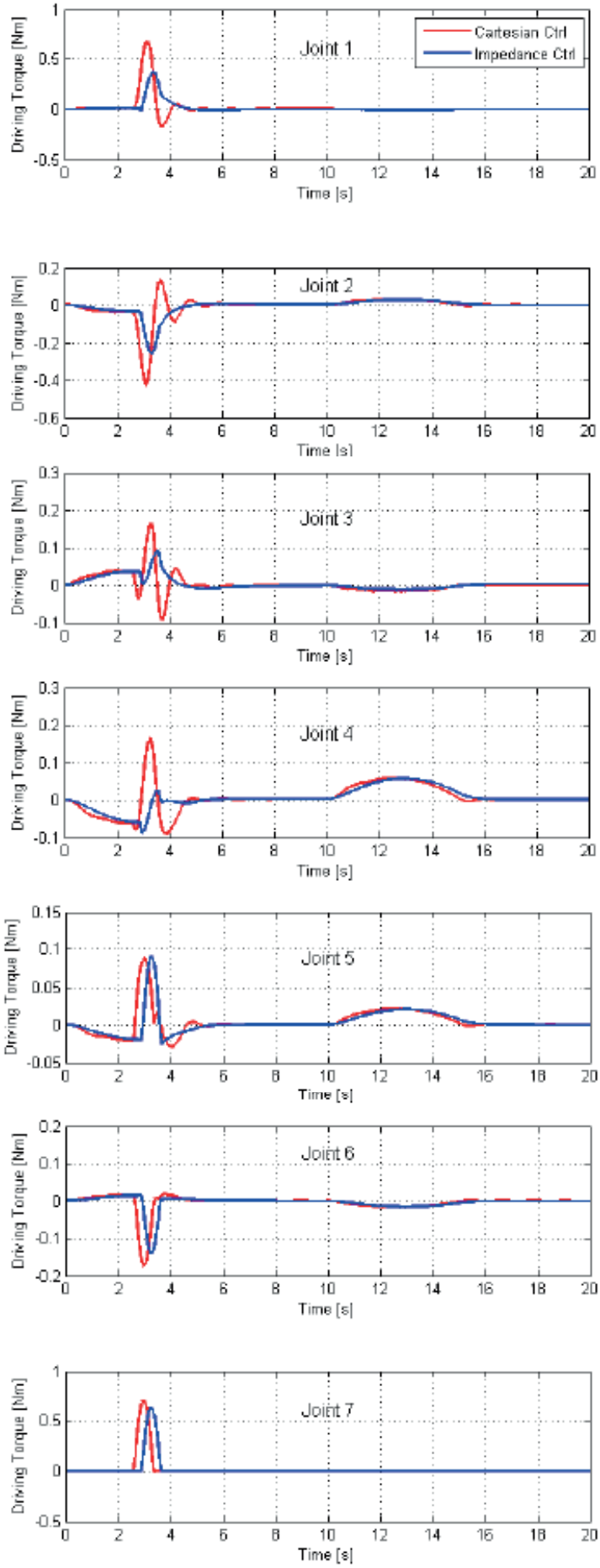

Fig. 8. Driving torques in simulation with 5 kg target
Rys. 8. Momenty w przegubach robota w przypadku kontaktu z obiektem-celem o masie 5 kg

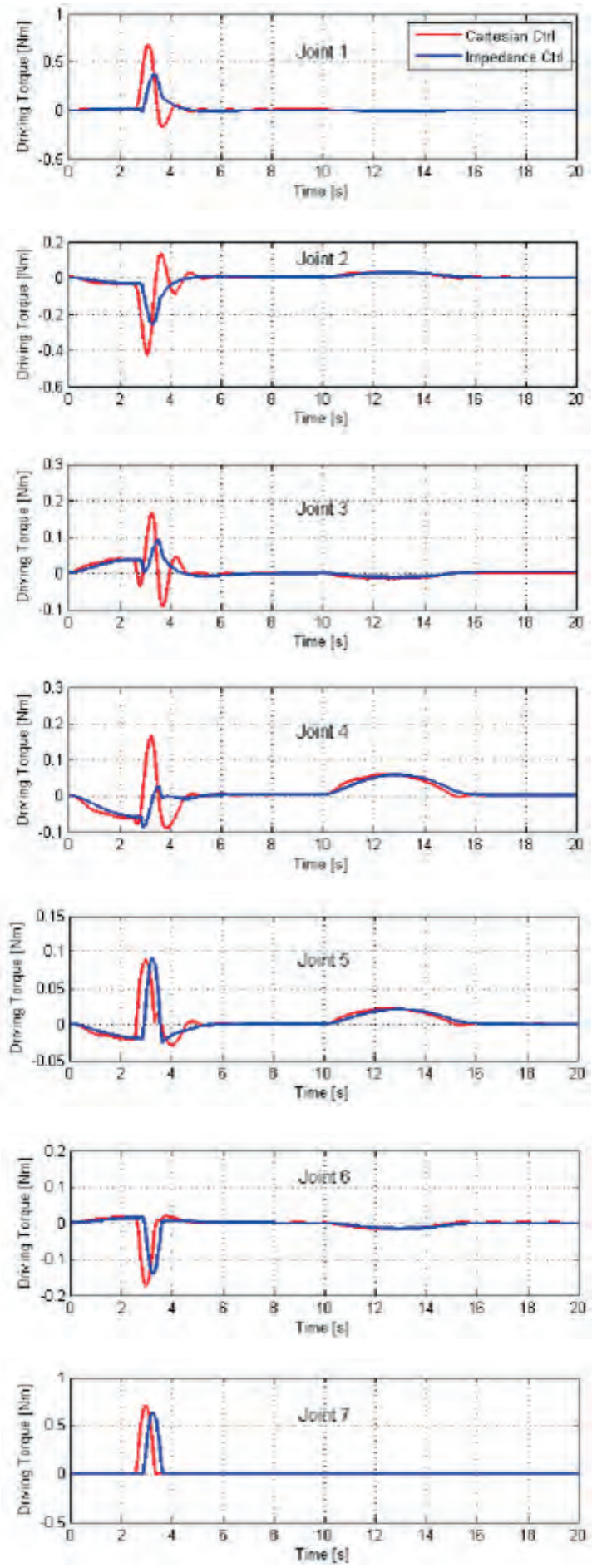

Fig. 9. Driving torques in simulation with 50 kg target
Rys. 9. Momenty w przegubach robota w przypadku kontaktu z obiektem-celem o masie 50 kg

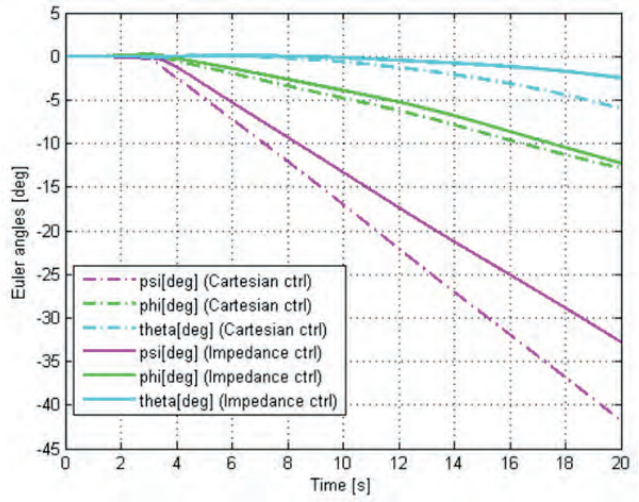

Fig. 10. Servicer orientation change for the 50 kg target case
Rys. 10. Zaburzenie orientacji bazy robota satlitarnego w przypadku kontaktu manipulatora robota z celem o masie 50 kg

The contact force $\boldsymbol{F}_{int}$ is proportional to the penetration depth d_{21} and contact stiffness k_k and its direction is determined by the unit vector $\boldsymbol{u}_{21}$.

$$\boldsymbol{F}_{int} = k_k \, d_{21} \, \boldsymbol{u}_{21} \tag{43}$$

The contact model parameter values are following: $k_k = 1000$ N/m, $r_1 = 10$ mm, $r_2 = 100$ mm. Two values of the free floating target mass were used in the simulation: 5 kg and 50 kg which results in different levels of reaction forces from the target in response to the push from the end effector. If another force acts on the robot end effector, it would add to the $\boldsymbol{F}_{int}$ and effectively enter the control torque via the dynamic Jacobian in the force interaction term of eq. (41).

4.3. Reference controller

Two simulation cases were executed: the impedance Controller (41) and the Cartesian controller (30). The configuration of the robot, the planned reference trajectory and the external disturbance force applied to the end effector were identical in both cases. In the impedance control scenario the following impedance parameters were used:

$$\boldsymbol{D} = 50 \, \boldsymbol{I}_{7\times 7}, \qquad \boldsymbol{E} = 50 \, \boldsymbol{I}_{7\times 7},$$

$$\boldsymbol{M}_d = \begin{bmatrix} 19.25 & 0 & 0 & 0 & 0 & 0 & 0 \\ 0 & 19.25 & 0 & 0 & 0 & 0 & 0 \\ 0 & 0 & 19.25 & 0 & 0 & 0 & 0 \\ 0 & 0 & 0 & 10 & 0 & 0 & 0 \\ 0 & 0 & 0 & 0 & 10 & 0 & 0 \\ 0 & 0 & 0 & 0 & 0 & 10 & 0 \\ 0 & 0 & 0 & 0 & 0 & 0 & 10 \end{bmatrix}$$

The symbol $\boldsymbol{I}_{7\times 7}$ denotes an identity matrix of the size given by the subscript. The matrix $\boldsymbol{M}_d$ describing the impedance in terms desired mass parameters is chosen such that the end effector behaves similarly to a rigid body with 10 % of the actual system's mass and inertia. The Cartesian controller used to obtain the benchmarking data uses the same gain values as in the work [15] with the matrix sizes adjusted to accommodate the seven joints of the robot simulated here.

$$\boldsymbol{G}_{\boldsymbol{\theta}} = 150 \boldsymbol{I}_{7\times 7}, \quad \boldsymbol{G}_{ee} = 100 \boldsymbol{I}_{7\times 7}$$

Table 2. Joint load comparison during contact with 5 kg target
Tabela 2. Zestawienie porównawcze obciążeń przegubów robota w przypadku kontaktu z celem o masie 5 kg. Wartości średniokwadratowe i szczytowe dla każdego przegubu

	RMS			PEAK		
Joint	**Impedance [N·m]**	**Cartesian [N·m]**	**Ratio* [%]**	**Impedance [N·m]**	**Cartesian [N·m]**	**Ratio* [%]**
1	0.01	0.013	76.9	0.103	0.124	83.1
2	0.018	0.02	90.0	0.088	0.095	92.6
3	0.013	0.014	92.9	0.063	0.063	100.0
4	0.03	0.031	96.8	0.083	0.073	113.7
5	0.011	0.011	100.0	0.022	0.033	66.7
6	0.008	0.008	100.0	0.032	0.039	82.1
7	0.014	0.015	93.3	0.185	0.202	91.6

Table 3. Joint load comparison during contact with 50 kg target
Tabela 3. Zestawienie porównawcze obciążeń przegubów robota w przypadku kontaktu z celem o masie 50 kg. Wartości średniokwadratowe i szczytowe dla każdego przegubu

	RMS			PEAK		
Joint	**Impedance [N·m]**	**Cartesian [N·m]**	**Ratio* [%]**	**Impedance [N·m]**	**Cartesian [N·m]**	**Ratio* [%]**
1	0.05	0.095	52.6	0.286	0.683	41.9
2	0.041	0.062	66.1	0.207	0.426	48.6
3	0.018	0.026	69.2	0.08	0.164	48.8
4	0.03	0.037	81.1	0.081	0.164	49.4
5	0.017	0.016	106.3	0.089	0.088	101.1
6	0.021	0.025	84.0	0.133	0.174	76.4
7	0.093	0.097	95.9	0.598	0.709	84.3

* The column "Ratio" shows the ratio of torque commanded by the impedance control to the torque due to Cartesian control, expressed as percentage of the Cartesian torque, for the same joint.

4.4. Simulation scenario

The controllers were fed the reference straight line trajectory leading from point a to b in the Cartesian space. The trajectory is visualized in Figure 5 the arrow.

The executed trajectory is designed such that the end effector must collide with the target mass. The duration of the simulation is designed to be 20 s. The planned trajectory timespan is 15 s. During the additional 5 s, the last point of the planned trajectory is used as a fixed reference point for the controller to track.

5. Results

The metrics useful for comparison of performance of the impedance controller and Cartesian controller are the driving torques in the robot joints, the ability to track the planned trajectory, the displacement of the base of the satellite from its initial state, in particular the change of its orientation, as this is what the satellites Attitude and Orientation Control System (AOCS) would need to account for. The Figure 6 shows the trajectory tracking results comparing the ability of the two controllers to follow a reference path when the target they collide with has a mass of 5 kg. The corresponding set of trajectory tracking plots for the case involving 50 kg target is shown in Figure 7. In the former case, the final tracking error is below 0.1 mm for both controllers, in the latter case the final tracking error for the Cartesian controller is 0.25 mm while for the impedance controller it is 1.6 mm, which is 1.6 % of the commanded displacement. In the view of the fact that the features which the manipulator tracks in order to grip them, are typically at least a few tens of millimetres in size [11], this result is considered to be a good performance. The reference orientation of the end effector is also included in the planned trajectory and kept is constant throughout the timespan of the simulation. The final orientation error was marginally low: 0.42° in the worst case, being the 50 kg target under impedance control. The Figure 8 and Figure 9 present the driving torques on each joint of the robotic manipulator. Those plots show that the impedance controller brings some qualitative advantages from the point of view of the AOCS of the satellite. During the transient after the collision which happens at $t = 2.5$ s, we observe that:

– The peak torque is lower for impedance controller than for the Cartesian one,
– The torque due to impedance control oscillates less, in particular, its change (slope) is slower, especially when the sign of the torque changes.

Those effects are more pronounced in case of the 50 kg target.

The closer a joint is to the satellite, the higher is the relative disturbance its torque causes to the satellite. Therefore, the lower and smoother the torques on joints 1, 2 and 3 is, the easier it is for the hypothetical AOCS system to account for it. The impedance controller brings this kind of an advantageous behaviour to the manipulator, which is clearly seen in the 50 kg target case. It is still present in the 5 kg case, although less pronounced.

The peak and RMS average of the joint driving torques are one set of potential useful shorthand metrics for the controllers' performance comparison. They allow to assess which control strategy leads to lower peaks and lower maximum transient loads across all joints.

The data in Table 2 shows the RMS and peak torques in the manipulator joints during contact with a 50 kg target. For all the joints except no. 5 the impedance controller shows both RMS averaged and peak loads lower than for the Cartesian controller. The torques in case of impedance controller do not exceed 52.6 % of the torques from Cartesian for the first joint of the robot, and in general, the loads on the joints closer to the satellite are lower. Still, for joint 5 the difference is marginal 1 %.

For the lighter target with mass 5 kg, the advantage of the impedance controller also prevails. The torques are closer to the ones from Cartesian controller, which is expected – in case of 5 kg target, the mass-like impedance components $\boldsymbol{M}_d$ of the manipulator system are roughly four times higher than that of the target – the controller makes the end effector act as if it was more difficult to be pushed off its intended trajectory which makes it more similar in behaviour to the Cartesian controller.

The contact with the target mass causes the free floating servicer satellite to exchange momentum and angular momentum with the target. As a result, the satellite starts to rotate and change its orientation. Again, from the perspective of assessment of controller's performance for a space application, the more favorable control strategy is the one that leads to lower magnitude of displacement and its time rate.

The Figure 10 shows the Euler angles of the satellite body which describe its orientation in inertial reference frame. By inspecting the slopes of the angles at the final time as well as their absolute values, it can be seen that the simulated impedance controller yielded a slower rotation of the servicer satellite.

6. Conclusions

The presented results of simulations comparing the impedance and a benchmark Cartesian controller show that the proposed impedance controller which takes into account the dynamic model of the satellite-robot system is able to drive the end effector to the planned target position with marginally higher error than Cartesian controller while doing so with substantially lower driving torques (and hence lower loads on the joints and their drives) for a target with mass about 50 % of the chaser satellite mass. This promising result is encouraging a further exploration of impedance control approaches to scenarios involving contact between the space robot manipulator and a target in future work.

References

1. Abiko S., Lampariello R., Hirzinger G., *Impedance control for a free-floating robot in the grasping of a tumbling target with parameter uncertainty.* [In:] 2006 IEEE/RSJ International Conference on Intelligent Robots and Systems, 1020–1025, DOI: 10.1109/IROS.2006.281785.
2. Basmadji F.L., Chmaj G., Rybus T., Seweryn K., *Microgravity testbed for the development of space robot, control systems and the demonstration of orbital maneuvers.* [In:] Proceedings of SPIE 11176, Photonics Applications in Astronomy, Communications, Industry, and High-Energy Physics Experiments 2019, DOI: 10.1117/12.2537981.
3. Basmadji F.L., Seweryn K., Sąsiadek J.Z., *Space robot motion planning in the presence of nonconserved linear and angular momenta.* „Multibody System Dynamics", Vol. 50, No. 1, 2020, 71–96, DOI: 10.1007/s11044-020-09753-x.
4. Bonnal C., Ruault J.-M., Desjean M.-C., *Active debris removal: Recent progress and current trends.* „Acta Astronautica", Vol. 85, 2013, 51–60, DOI: 10.1016/j.actaastro.2012.11.009.
5. Echeandia S., Wensing P.M., *Numerical methods to compute the Coriolis matrix and Christoffel symbols for rigid--body systems.* „Journal of Computational and Nonlinear Dynamics", Vol. 16, No. 9, 2021, DOI: 10.1115/1.4051169.
6. ESA Space Debris Office, *ESA's annual space environment report.* Darmstadt.
7. Hogan N., *Impedance control of industrial robots.* „Robotics and Computer-Integrated Manufacturing", Vol. 1, No. 1, 1984, 97–113, DOI: 10.1016/0736-5845(84)90084-X.
8. Hogan N., *Impedance Control: An Approach to Manipulation*, [In:] 1984 American Control Conference, 304–313, DOI: 10.23919/ACC.1984.4788393.
9. Lu W.-S., Meng Q.-H., *Impedance control with adaptation for robotic manipulations*, „IEEE Transactions on Robotics and Automation", Vol. 7, No. 3, 1991, 408–415, DOI: 10.1109/70.88152.
10. Luu M.A., Hastings D.E., *Review of on-orbit servicing considerations for low-earth orbit constellations.* Accelerating Space Commerce, Exploration, and New Discovery Conference, ASCEND 2021, DOI: 10.2514/6.2021-4207.
11. Oleś J., Rybus T., Seweryn K., Surowiec M., Wojtyra M., Pietras M., Scheper M., *Testing and simulation of contact during on-orbit operations.* [In:] Proceedings of 14th Symposium on Advanced Space Technologies in Robotics and Automation (ASTRA'2017). European Space Agency.
12. Palma P., Seweryn K., *Space robot equipped with compliant linear actuator on end effector: simulations results.* [In:] R.S. Romaniuk, L. Maciej (Eds.), Proceedings of SPIE 11176, Photonics Applications in Astronomy, Communications, Industry, and High-Energy Physics Experiments 2019, DOI: 10.1117/12.2537207.
13. Papadopoulos E.G., *Nonholonomic Behaviour in Free--floating Space Manipulators and its Utilization.* „Nonholonomic Motion Planning", 1993, 423–445, DOI: 10.1007/978-1-4615-3176-0_11.
14. Rybus T., Seweryn K., *Trajectory Planning and Simulations of the Manipulator Mounted on a Free-Floating Satellite*, „Aerospace Robotics, 2013, 61–73, DOI: 10.1007/978-3-642-34020-8_6.
15. Rybus T., Seweryn K., Sąsiadek J.Z., *Control System for Free-Floating Space Manipulator Based on Nonlinear Model Predictive Control* (*NMPC*), „Journal of Intelligent and Robotic Systems: Theory and Applications", Vol. 85, 2017, 491–509, DOI: 10.1007/s10846-016-0396-2.
16. Rybus T., Wojtunik M., Basmadji F.L. (2022). *Optimal collision-free path planning of a free-floating space robot*

using spline-based trajectories. „Acta Astronautica", Vol. 190, 2022, 395–408, DOI: 10.1016/j.actaastro.2021.10.012.
17. Sakai S., *An Exact Impedance Control of DC Motors Using Casimir Functions*, Ferroelectrics. InTech, Dec. 14, 2010. DOI: 10.5772/13432.
18. Seweryn K., *Dynamika manewru zbliżania satelitów i ich połączenia za pomocą manipulatora o więzach nieholonomicznych*. Politechnika Warszawska, 2008.
19. Seweryn K., Banaszkiewicz M., *Optimization of the trajectory of a general free-flying Guidance, manipulator during the rendezvous manoeuvre*. [In:] Proceedings of the AIAA navigation and control conference and exhibit. Honolulu, Hawaii, USA, 2008, DOI: 10.2514/6.2008-7273.
20. Sharma S., Suomalainen M., Kyrki V., *Compliant Manipulation of Free-Floating Objects*, [In:] Proceedings of IEEE International Conference on Robotics and Automation, 2018, 865–872, DOI: 10.1109/ICRA.2018.8462889.
21. Song P., Yu Y., Zhang, X. (2019). A Tutorial Survey and Comparison of Impedance Control on Robotic Manipulation. Robotica, 37(5), 801–836.
22. Tchoń K., *Dystrybucje w robotyce*, Krynica-Zdrój 2014, Internal presentation of Instytut Informatyki, Automatyki i Robotyki Politechniki Wrocławskiej.
23. Umetani Y., Yoshida K., *Resolved Motion Rate Control of Space Manipulators with Generalized Jacobian Matrix*. „IEEE Transactions on Robotics and Automation", Vol. 5, No. 3, 1989, 303–314, DOI: 10.1109/70.34766.
24. United Nations; *Technical Report on Space Debris*. United National Publication, 1999.
25. Yoshida K., Nakanishi H., Inaba N., Ueno H., Oda M., *Contact Dynamics and Control Strategy Based on Impedance Matching for Robotic Capture of a Non-cooperative Satellite*, „Advanced Robotics", Vol. 18, No. 2, 2004, 175–198.

Zastosowanie sterowania impedancyjnego robotem kosmicznym typu free-floating w kontekście usuwania śmieci kosmicznych

Streszczenie: Wiele obiektów orbitujących Ziemię stanowią wyeksploatowane lub nieczynne satelity i inne urządzenia kosmiczne oraz ich fragmenty. Poruszając się w sposób niekontrolowany po orbitach aktywnie wykorzystywanych stanowią zagrożenie dla czynnych satelitów, stacji kosmicznej, astronautów jak i również rakiet wynoszących w przestrzeń kosmiczną nowe satelity. Obiekty te uznawane są za śmieci kosmiczne. Zdolność chwycenia i manipulowania niewspółpracującym obiektem na orbicie Ziemi przez robota satelitarnego pozwoliła by na zmniejszenie liczby śmieci kosmicznych i zagrożeń z nimi związanych w dwojaki sposób:
po pierwsze umożliwiła by chwycenie i usunięcie śmieci kosmicznych znacznej wielkości z orbity,
po drugie dała by możliwość serwisowania i tym samym przedłużenia okresu eksploatacyjnego satelitów będących blisko końca swojej nominalnej misji, zapobiegając by stały się one śmieciami kosmicznymi. Oba te zastosowania wymagają fizycznego wejścia w kontakt pojazdu kosmicznego chwytającego oraz obiektu chwytanego. W naziemnych zastosowaniach robotów, w których dochodzi do kontaktu manipulatora robota z otoczeniem, powszechnie stosowane są metody sterowania impedancyjnego. W niniejszym tekście autorzy proponują wykorzystanie sterowania impedancyjnego w oparciu o model (model-based impedance control) do realizacji manewru wejścia w kontakt końcówki manipulatora robota satelitarnego z niewspółpracującym obiektem w stanie nieważkości. W pracy przedstawiono wyprowadzenie prawa sterowania impedancyjnego manipulatorem o swobodnej bazie w oparciu o model, z wykorzystaniem jakobianu uogólnionego (Generalized Jacobian Matrix, GJM), oraz rezultaty symulacji manewru wejścia końcówki roboczej manipulatora kosmicznego w kontakt z nieważkim obiektem. Wyniki symulacji pokazują, że zaproponowane prawo sterowania pozwala realizować zadanie śledzenia trajektorii zachowując momenty i obciążenia w przegubach robota na niskim poziomie.

Słowa kluczowe: robot kosmiczny, manipulator orbitalny, sterowanie impedancyjne, naprawa urządzeń na orbicie, usuwanie śmieci kosmicznych, robotyka

Piotr Palma, PhD, Eng.

piotr@palmaline.pl, ppalma@cbk.waw.pl
ORCID: 0000-0001-7604-8834

Received his PhD from Space Research Centre of Polish Academy of Science (CBK PAN) in the discipline of Automation, Electronics, Electrical Engineering and Space Technology in 2023. His scope of research covers space robotics, machine learning, dynamics and control systems, nonlinear control particularly in the context of engineering applications of impedance control and advanced actuators. He graduated with MSc from Coventry University, UK and Technical University of Lodz, Poland in mechanical engineering and applied computer science. Additionally Piotr Palma has been involved in development of hardware systems for space missions..

Tomasz Rybus, PhD, Eng.

trybus@cbk.waw.pl
ORCID: 0000-0002-7957-5346

Received his Ph.D. in Automation and Robotics from Wrocław University of Science and Technology in 2017. He is currently employed as an Assistant Professor at the Space Research Centre of the Polish Academy of Sciences (CBK PAN) in Warsaw. His research interests include the dynamics and control of satellite-manipulator systems. Additionally, he is actively engaged in experimental validation of robotic systems in simulated microgravity conditions. Tomasz Rybus has been involved in several European Space Agency and national projects related to these topics, and he has participated in the e.Deorbit mission consolidation phase study..

Prof. Karol Seweryn, DSc, PhD, Eng.

kseweryn@cbk.waw.pl
ORCID: 0000-0002-4372-0900

Assistant professor at the Space Research Centre of the Polish Academy of Sciences, Warsaw, Poland. In 2008 received the Ph.D. from Warsaw University of Technology, Faculty of Power and Aeronautical Engineering in the field of Robotics. In 2017 received the Doctor of Science degree from AGH University of Science and Technology, Faculty of Mechanical Engineering and Robotics in the field of Robotics. In recent years he has been involved in more than 20 projects, including ESA e.deorbit mission, PACKMOON sampling tool development for ESA, Project manager of the CHOMIK sampling tool development for Phobos-Grunt mission and Co-I of the on-going STIX project for ESA Solar Orbiter mission. Currently his research is focused on the dynamics and control algorithms of space robots as well as on the development of mechatronic devices for In Situ Resource Utilization (ISRU) activities.